Supporting Information for

Venus' Mass Spectra Show Signs of Disequilibria in the Middle Clouds

Rakesh Mogul[1*], Sanjay S. Limaye[2], M. J. Way[3,4,5], Jaime A. Cordova[6]

[1] Chemistry & Biochemistry Department, California State Polytechnic University, Pomona, CA, USA
[2] Space Science and Engineering Center, University of Wisconsin, Madison, WI, USA
[3] NASA Goddard Institute for Space Studies, 2880 Broadway, New York, NY, USA
[4] GSFC Sellers Exoplanet Environments Collaboration, Greenbelt, MD, USA
[5] Theoretical Astrophysics, Department of Physics and Astronomy, Uppsala University, Uppsala, Sweden
[6] Laboratory of Genetics, University of Wisconsin, Madison, WI, USA

***Corresponding author:** Rakesh Mogul (rmogul@cpp.edu)

Contents of this file:

Supplemental Methods

Assignments and Fragmentation Patterns

Changes to the pre-selected mass values (apparent amu) during operation in the clouds were estimated by tracking pre-selected values that were identical to the exact masses for CH_3^+, H_2O^+, CO^+, and $^{136}Xe^+$, and similar (≤0.003 amu) to the exact masses for N_2^+ and $^{40}Ar^+$. Exact masses for CH_3^+ and H_2O^+ were calculated using a mass of 1.0079 amu for hydrogen, per measurements that were published in 1976 (*Roth et al.*, 1976) before launch of the Pioneer-Venus Large Probe in 1978. Shifts to the pre-selected masses ranged from 0.001-0.007 amu at 51.3 km, 0.000-0.009 amu at 55.4 km, 0.000-0.030 amu at 58.3 and 59.9 km, 0.001-0.023 amu at 61.9 km, and 0.001-0.021 amu at 64.2 km. In practice, we used the maximum shift to assist in sorting initial chemical assignments, where pre-selected masses that differed (absolute) from the expected masses by less than the maximum shift were roughly treated as near-centroids (or near the peak means); while pre-selected values that differed from exact masses by less than the estimated FWHM of the target species were treated as components of the sloping edges of the peak (off-set peak). In turn, regressions to mass pairs and triplets for target species of <40 amu were constrained using the target exact mass and a variance that equaled the averaged Δamu between 15-40 amu (CH_3^+, H_2O^+, CO^+, N_2^+, & $^{40}Ar^+$) at each resepective altitude, along with the estimated FWHM and standard deviation, which was obtained by linear regression at the resepective altitude (similar to **Figure 1H**). Regressions to single mass points, given the uncertainty in the pre-selected mass value, were only used to obtain rough estimates of the calculated maximum counts.

Isobaric species were additionally disambiguated using isotope ratios. Abundances for $^{13}CO^+$ were obtained using the $^{13}C/^{12}C$ ratio ($1.33x10^{-2} \pm 0.01x10^{-2}$) and counts of CO^+ from simulated spectra (**Figure 1D** & **S1**); in turn, subtraction of $^{13}CO^+$ from the maximum counts at 29 amu provided abundances for $^{14}N^{15}N$. When considering N_2^+ abundances from simulated spectra, this provided a $^{15}N/^{14}N$ ratio of $2.63x10^{-3} \pm 0.86x10^{-3}$ across the altitudes of 61.2-51.3 km ($^{14}N^{15}N$ was below the limit of detection at 64.2 km). For NO^+, counts were obtained by (1) using counts for CO^+ from simulated plots (**Figure S1** legend), (2) converting to counts for $C^{18}O^+$ using the $^{18}O/^{16}O$ isotope ratio ($2.18x10^{-3} \pm 0.17\ x10^{-3}$), and (3) constraining regressions to the mass pair at 30 amu (for NO^+, $C^{18}O^+$, and $C_2H_6^+$) using the calculated counts of $C^{18}O^+$, estimated FWHM values, and expected masses. Similarly, maximum possible counts for NO_2^+ ($\leq$620) were estimated using the error in the $^{18}O/^{16}O$ ratio.

Fragmentation patterns for CO_2, HNO_2, and H_2SO_4 are displayed in **Figures S3-4**. Mass data for parent ions and associated species were binned and plotted against reference spectra obtained from the NIST Chemistry WebBook (https://webbook.nist.gov/chemistry/) (*Wallace*, 2020), MassBank Europe (https://massbank.eu/MassBank/), PubChem (https://pubchem.ncbi.nlm.nih.gov), or from published reports.

Organic Contamination

Per *Hoffman et al.* (1980a), pre-flight studies with the LNMS revealed mass signals at 77 and 78 amu that were attributed to benzene arising from the vacuum sealants. Unfortunately, we are aware of no technical reports that describe contamination control for the LNMS. It is also possible that components of the LNMS were cleaned with trichloroethylene (TCE; C_2HCl_3) and/or treated with a sealant such as Vacseal® High Vacuum Leak Sealant, which contains TCE, xylene, and ethyl benzene. After assembly, but pre-launch, the LNMS was also possibly subjected to ~750 K for an unknown amount of time to remove organics.

When at Venus, the LNMS performed five complete peak-stepping operations in the upper atmosphere with data collection beginning at 64.2 km. Across the cloud measurements, however, counts and mass values were suggestive of the presence of the TCE parent ion (129.914383 amu), $C_2HCl_3^+$ (M^+), along with the ions of $(M+2)^+$, $[M\text{-}Cl]^+$, $[(M+2)\text{-}Cl]^+$, and possibly $[M\text{-}2Cl]^+$. The spread in counts, however, were not consistent with terrestrial $^{37}Cl/^{35}Cl$ ratios, which implied the presence of entangled isobaric species.

Per *Donahue et al.* (1981), these same mass positions (**128.905**, **129.921**, **130.914**, and **131.922 amu**) were assigned to ^{129}Xe, ^{130}Xe, ^{131}Xe, and ^{132}Xe, which suggested that contamination by TCE was considered to be minimal by the original investigators. Nevertheless, in the event of low-level TCE contamination, then the counts of 5 for the parent ion, $C_2HCl_3^+$, were suggestive of TCE being a minor source of atomic chlorine (Cl^+). Per the NIST reference, atomic chlorine is ~10% of the TCE parent ion (base peak), which amounted to hypothetical counts of ~0.5 for atomic chlorine arising from TCE. Reference spectra also indicated that $C_2H_6^+$ and $C_2H_4^+$ – which were potential assignments in the data – were not products of TCE fragmentation.

Evaluation of the NIST reference spectra for *o*-xylene, *m*-xylene, *p*-xylene, and ethyl benzene, indicated that benzene and benzyl radical cations were produced in yields of ~10 and 15% of the base peak (tropylium, $C_7H_7^+$; 91.054775 amu). In the LNMS data, the pre-selected value **78.053 amu** was consistent with the mass of benzene ($C_6H_6^+$), while the counts of 16 implied the presence of a substantially larger base peak and parent ion. However, the LNMS did not sample masses for the xylene and tropylium ions. Again, in the absence of technical information, we are unable to discern between contaminants or the atmosphere as a source of the counts at **78.053 amu**.

We posit that a majority of the residual sealant may have been sufficiently removed by the pre-launch and pre-data acquisition preparations – as may have been the case for TCE. If so, the massive increase at **78.053 amu** to ~30,000 counts at 14-15 km (well below the clouds) may be indicative of alternative chemical species such as dimethyl sulfoxide (DMSO; $(CH_3)_2SO$) or chemical fragments such as P_2O^+. In support of this assessment are counts at **78.924 amu**, which likely represent the ^{13}C-benzene isotopologue, $C_5{}^{13}CH_6$ (79.050305 amu). In sharp contrast to benzene, counts at this position did not exhibit the massive increase at 14-15 km. Moreover, the relative counts at **78.924**, **78.053**, and **77.040 amu** across the altitude profile were inconsistent with the relative abundances of $C_6H_5^+$, $C_6H_6^+$, and $C_5{}^{13}CH_6^+$ from the NIST and MassBank references for benzene. Instead, adjustments using the NIST reference provided a maximum of ~870 counts for benzene below the clouds, which was well below the measured counts of ~30,000. At 51.3 km, adjustments of the counts at **78.924** (2), **78.053** (16), and **77.040** (1) **amu** were suggestive of maximum values of ~2 counts for $C_6H_5^+$, ~7 counts for $C_6H_6^+$ (benzene), and ~0.5 counts for $C_5{}^{13}CH_6^+$.

Table S1. List of parent ions and fragmentation products for (A) CO_2, (B) PH_3, (C) H_2S, (D) HNO_2 and HNO_3, (E) $H^{35}Cl$ and $H^{37}Cl$, (F) fragments of H_2SO_4, (G) NH_3, and (H) low-mass organics; where measured counts at the pre-selected masses or calculated (*) counts from simulated spectra are listed.

(A) *carbon dioxide & carbon monoxide* (CO_2 & CO)

apparent amu	count	formula	parent & fragment ions	expected mass
45.995	7936	$CO^{18}O^+$	$(M+2)^+$	45.994160
44.991	21504	$^{13}CO_2^+$	$(M+1)^+$	44.993355
43.991	1769472	CO_2^+	M^+	43.990000
28.997	6656	$^{13}CO^+$	CO: $(M+1)^+$ CO_2: $[(M+1)\text{-}O]^+$	28.998355
29.997	801*	$C^{18}O^+$	CO: $(M+2)^+$ CO_2: $[(M+2)\text{-}O]^+$	29.999160
27.995	423535*	CO^+	CO:M^+ CO_2: $[M\text{-}O]^+$	27.995000
22.496	560	$^{13}CO_2^{++}$	$(M+1)^{++}$	22.496677
21.995	47104	CO_2^{++}	M^{++}	21.995000
15.995	335872	O^+	CO: $[M\text{-}C]^+$ CO_2: $[M\text{-}O\text{-}C]^+$	15.995000
12	344064	$^{12}C^+$	CO: $[M\text{-}O]^+$ CO_2: $[M\text{-}2O]^+$	12.000000

(B) *phosphine* (PH_3)

apparent amu	count	formula	parent & fragment ions	expected mass
35.005	6*	$^+PH_2D$	$(M+1)^+$	35.003659
33.992	19*	$^+PH_3$	M^+	33.997382
32.985	15*	$^+PH_2$	$[M\text{-}H]^+$	32.989557
30.973	6*	P^+	$[M\text{-}3H]^+$	30.973907

(C) *hydrogen sulfide* (H_2S)

apparent amu	Count	formula	parent & fragment ions	expected mass
34.005	7*	HDS^+	$(M+1)^+$	33.993998
33.992	1.7*	H_2S^+	M^+	33.987721
32.985	2*	HS^+	$[M\text{-}H]^+$	32.979896
31.972	≤8*	$^{32}S^+$	$[M\text{-}2H]^+$	31.972071

(D) *nitrous & nitric acid* (HNO_2 & HNO_3)

apparent amu	count	formula	parent & fragment ions	expected mass
62.994	1	HNO_3^+	HNO_3: M^+	62.995899
47.000	94	HNO_2^+	HNO_2: M^+	47.000899
45.995	≤620*	NO_2^+	HNO_3: $[M\text{-}17]^+$	45.993074

31.006	26	HNO^+	HNO_2: $[M-16]^+$	31.005899
29.997	≤208*	NO^+	HNO_3: $[M-33]^+$ HNO_2: $[M-17]^+$	29.998074
17.002	296	^+OH	HNO_3: $[M-46]^+$ HNO_2: $[M-30]^+$	17.002825
15.995	335872	O^+	HNO_3: $[M-47]^+$ HNO_2: $[M-31]^+$	15.995000
14.000	19456	$^{14}N^+$	HNO_3: $[M-49]^+$ HNO_2: $[M-33]^+$	14.003074
(E) ***hydrochloric acid*** **(HCl)**				
apparent amu	**count**	**formula**	**parent & fragment ions**	**expected mass**
37.968	36*	$H^{37}Cl^+$	$(M+2)^+$	37.973728
36.966	6*	$^{37}Cl^+$	$[(M+2)-H]^+$	36.965903
35.981	4*	HCl^+	M^+	35.976678
34.972	12*	$^{35}Cl^+$	$[M-H]^+$	34.968853
1.008	3520	H^+	$[M-Cl]^+$ & $[(M+2)-Cl]^+$	1.007825
(F) ***sulfuric acid fragments*** **(H_xSO_y; x = 0-2, y = 1-3)**				
apparent amu	**count**	**formula**	**parent & fragment ions**	**expected mass**
79.958	0	SO_3^+	$[M-18]^+$	79.957071
65.961	0.3*	$^{34}SO_2^+$	$[(M+2)-34]^+$	64.961459
64.96	3	HSO_2^+	$[M-33]^+$	64.969896
63.962	5	SO_2^+	$[M-34]^+$	63.962071
50.969	0.1*	$H^{34}SO^+$	$[(M+2)-49]^+$	50.970692
49.968	3	$^{34}SO^+$	$[(M+2)-50]^+$	49.962867
48.974	2	$^{33}SO^+$	$[[(M+1)-50]^+$	48.966459
47.966	10	SO^+	$[M-50]^+$	47.967071
(G) ***ammonia*** **(NH_3)**				
apparent amu	**count**	**formula**	**parent & fragment ions**	**expected mass**
18.034	≤20*	NH_2D^+	M^+	18.032826
16.018	40960	$^+NH_2$	$[M-2H]^+$	16.018724
15.013	7680	^+NH	$[M-3H]^+$	15.010899
14	19456	$^{14}N^+$	$[M-4H]^+$	14.003074
(G) ***low-mass organics*** **(C_xH_y)**				
apparent amu	**count**	**formula**	**parent & fragment ions**	**expected mass**
78.924	~0.5*	$C_5(^{13}C)H_6^+$	^{13}C-Benzene: $(M+1)^+$	78.046950
78.053	~7*	$C_6H_6^+$	Benzene: M^+	78.046950
77.04	~2*	$C_6H_5^+$	Benzene F1: $[M-H]^+$	77.039125
40.029	80	$C_3H_4^+$	Propyne: M^+	40.031300

30.046	≤100*	$C_2H_6^+$	Ethane: M^+	30.046950
29.039	992	$C_2H_5^+$	Ethane F1: $[M\text{-}H]^+$	29.039125
28.032	122880	$C_2H_4^+$	Ethene: M^+ Ethane F2: $[M\text{-}2H]^+$	28.031300
27.023	≤50*	$C_2H_3^+$	Ethene F1: $[M\text{-}H]^+$ Ethane F3: $[M\text{-}3H]^+$	27.023475
26.014	≤10*	$C_2H_2^+$	Ethene F2: $[M\text{-}2H]^+$ Ethane F4: $[M\text{-}4H]^+$ Ethyne: M^+	26.015650
16.031	39936	CH_4^+	Methane: M^+	16.031300
15.023	22528	CH_3^+	Methane F1: $[M\text{-}H]^+$ Ethane F5: $[M\text{-}3H\text{-}C]^+$	15.023475

*Calculated or estimated from simulated spectra and/or adjusted using isotope ratios or relative abundances from reference spectra.

Table S2

Isotope Ratios				
Isotopes	**Venus**	**Altitudes**	**Comments**	**Earth**
$^{13}C/^{12}C$	$1.33 \times 10^{-2} \pm 0.01 \times 10^{-2}$	64.2-51.3 km & 23.0-0.9 km	Clog excluded (50.3-24.4 km); $1.28 \times 10^{-2} \pm 0.02 \times 10^{-2}$ was obtained across all altitudes.	1.08×10^{-2}
$^{15}N/^{14}N$	$2.63 \times 10^{-3} \pm 0.86 \times 10^{-3}$	59.9-51.3 km	$^{14}N^{15}N_2^+$ was below the detection limit at 64.2 km; and ratio was not calculated <51.3 km.	3.65×10^{-3}
$^{18}O/^{16}O$	$2.18 \times 10^{-3} \pm 0.17 \times 10^{-3}$	64.2-51.3 km & 23.0-0.9 km	Clog excluded (50.3-24.4 km); $2.14 \times 10^{-3} \pm 0.26 \times 10^{-3}$ was obtained across all altitudes.	2.05×10^{-3}
$^{33}S/^{32}S$	$1.4 \times 10^{-2} \pm 0.9 \times 10^{-2}$	39.3-25.9 km	During the clog where respective counts were enriched.	7.88×10^{-3}
$^{34}S/^{32}S$	$5.8 \times 10^{-2} \pm 0.7 \times 10^{-2}$	39.3-25.9 km	During the clog where respective counts were enriched.	4.39×10^{-2}
$^{37}Cl/^{35}Cl$	$4.5 \times 10^{-1} \pm 0.7 \times 10^{-1}$	58.3-51.3 km	$^{37}Cl^+$ was below the detection limit >58.3 km; and ratio not calculated <51.3 km.	3.20×10^{-1}

Figure S1

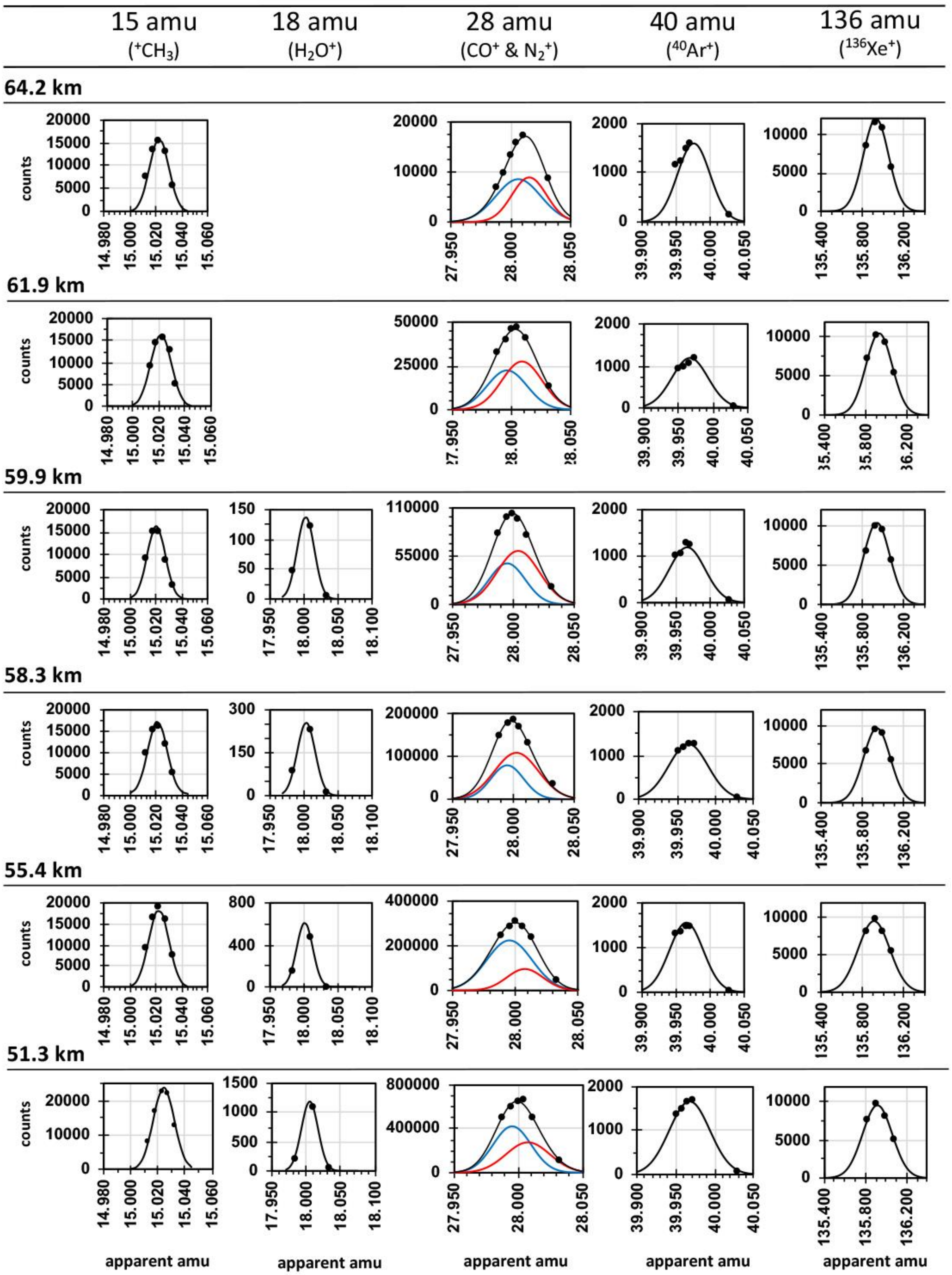
15 amu
($^{+}CH_3$)
18 amu
(H_2O^+)
28 amu
(CO^+ & N_2^+)
40 amu
($^{40}Ar^+$)
136 amu
($^{136}Xe^+$)
64.2 km
61.9 km
59.9 km
58.3 km
55.4 km
51.3 km
counts
apparent amu

Figure S1. Gaussian fits to the mass peaks at 15 (CH_3^+), 18 (H_2O^+), 28 (CO^+ & N_2^+), 40 ($^{40}Ar^+$), and 136 ($^{136}Xe^+$) amu across the altitudes of 64.2, 61.9, 59.9, 58.3, 55.4, and 51.3 km. Error bars (y-axis) are smaller than the marker size of the data points. For water (18 amu), counts at 17.985 amu were corrected for $^{36}Ar^{++}$ using yields from the NIST mass spectral reference for Ar (and counts for $^{36}Ar^+$); poor fits were obtained at 61.9 and 64.2 km due to relatively higher abundances of $^{36}Ar^{++}$. For 28 amu, contributions from isobaric CO^+ and N_2^+ were included. For 15, 40, and 136 amu, regressions were minimized using least squares; and for 18 and 28 amu, regressions were minimized by least absolute deviations (LAD). Regressions for CO^+ & N_2^+ (51.3 km) provided solutions ranging from ~40-60% CO^+ and N_2^+, where the solution of ~60% CO^+ and ~40% N_2^+, which is plotted in this Figure, providing the lowest relative summed absolute deviation (SAD); the lower solution of 40% CO^+ was used to calculate upper abundances of NO^+ in **Section 3.3**.

Figure S2

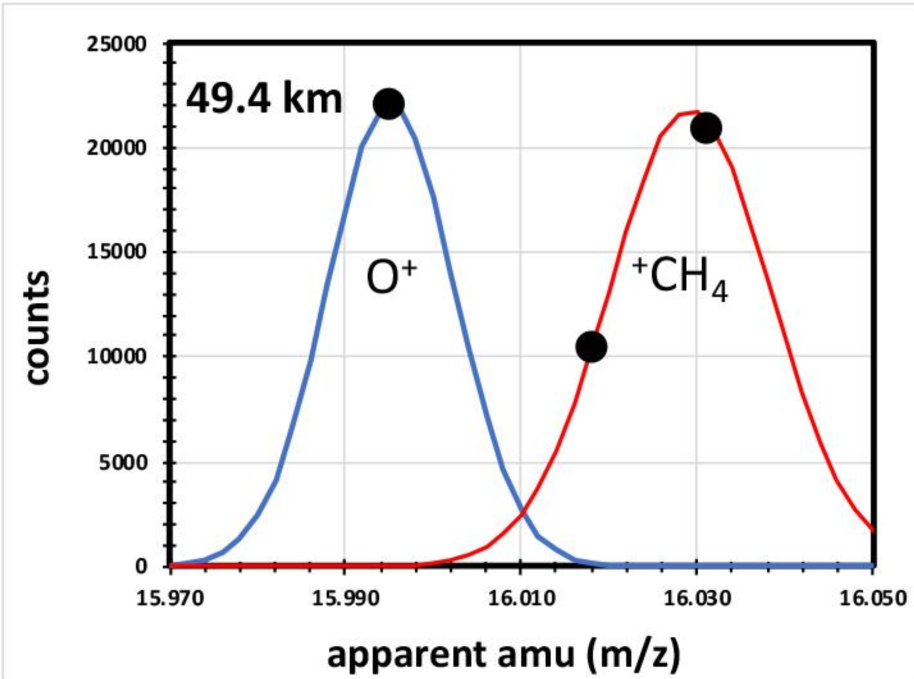

Figure S2. Example fit to the LNMS data at 16 amu for O^+ and CH_4^+ at 49.4 km; at this altitude, counts are roughly equal, thereby allowing calculation of resolving power between the mass pairs, which was 471 with a 12% valley minima for O^+.

Figure S3

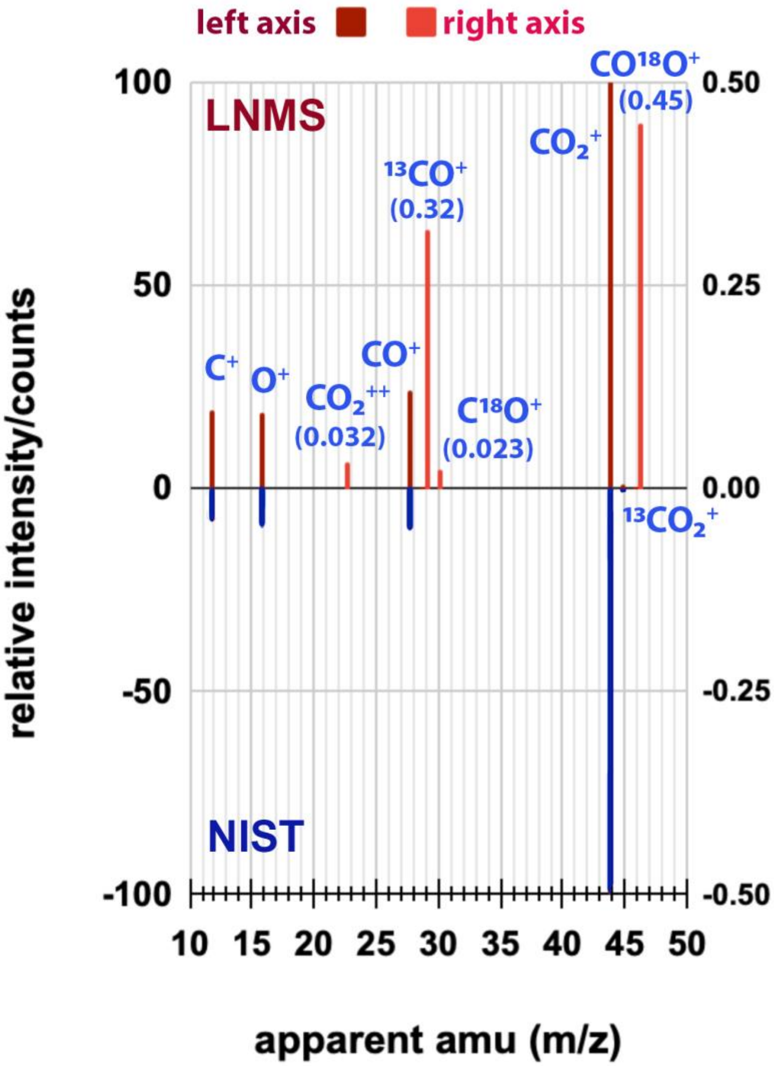

Figure S3. Comparison of the fragmentation pattern for CO_2 from the LNMS data (maroon, positive quadrant) and the NIST mass spectral reference (blue, negative quadrant); corrected CO^+ abundances were obtained from simulated spectra, CO_2^{++}, $C^{18}O^+$, and $C^{16}O^{18}O^+$ are plotted on the left-hand y-axis, and masses were displayed using unit resolution for clarity.

Figure S4

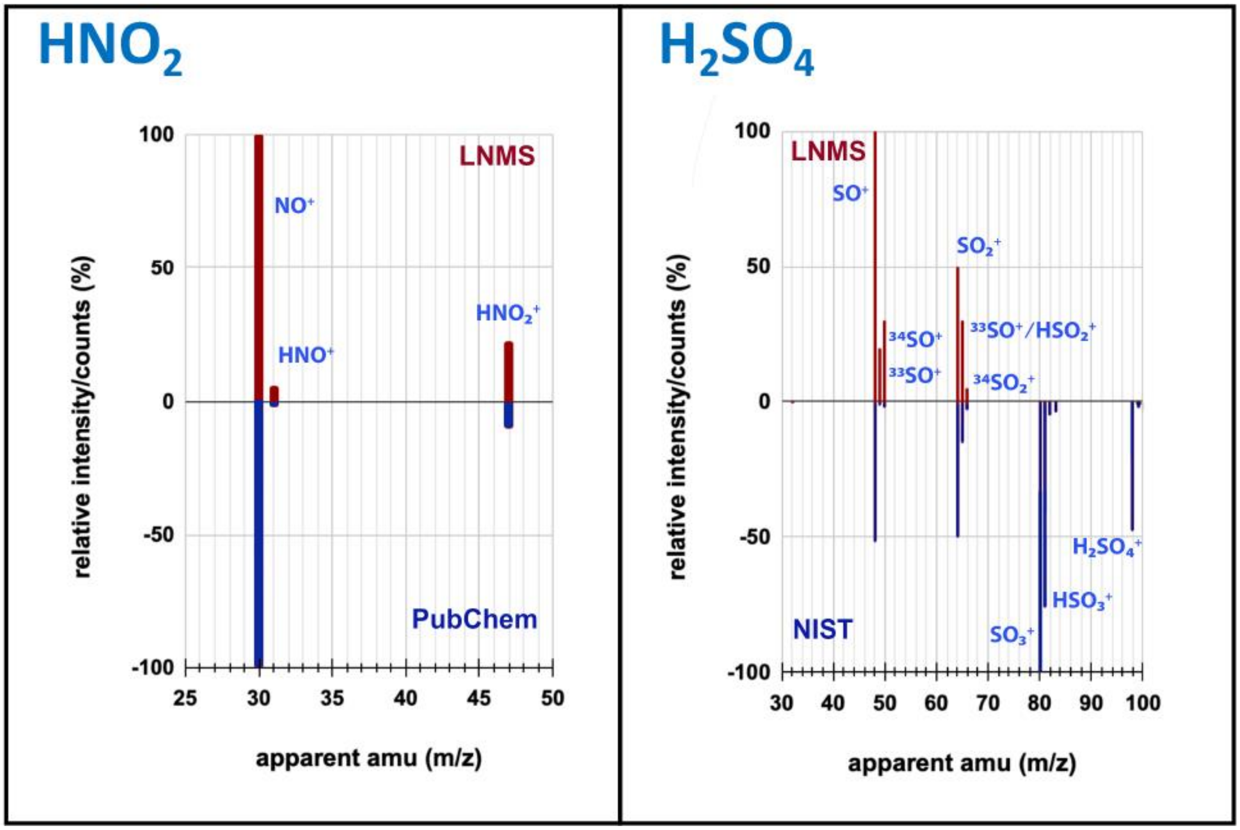

Figure S4. Comparison of fragmentation patterns for HNO_2 and H_2SO_4 from the LNMS data (maroon, positive quadrant) and the PubChem and NIST mass spectral references (blue, negative quadrant); masses were displayed using unit resolution for clarity, and relative scales do not reflect the error in the low counts for all potential H_2SO_4 fragments.